Physics of the Earth and Planetary Interiors 183 (2010) 151–163

Contents lists available at ScienceDirect

Physics of the Earth and Planetary Interiors

journal homepage: www.elsevier.com/locate/pepi

Grainsize-sensitive viscoelastic relaxation in olivine: Towards a robust laboratory-based model for seismological application

Ian Jackson[a,*], Ulrich H. Faul[b]

[a] Research School of Earth Sciences, Australian National University, Canberra, ACT 0200, Australia
[b] Department of Earth Sciences, Boston University, Boston, MA, USA

ARTICLE INFO

Article history:
Received 31 August 2009
Received in revised form 7 July 2010
Accepted 10 September 2010

Guest Editors
Daisuke Suetsugu
Craig Bina
Toru Inoue

Editor
Mark Jellinek

Keywords:
Viscoelastic relaxation
Seismic-wave attenuation
Seismic wave-speeds
Grain-boundary sliding
Grain size

ABSTRACT

Torsional forced oscillation data for a newly prepared specimen of dry, melt-free polycrystalline Fo_{90} olivine of 3.1 μm average grainsize have been used to reassess alternative strategies for the parameterisation of grainsize-sensitive viscoelastic relaxation. Our previously employed extended Burgers model has been modified by prescribing anharmonic temperature and pressure dependence of the effective unrelaxed shear modulus G_U relative to its value G_{UR} at reference values of temperature (T_R = 900 °C) and pressure (P_R = 0.2 GPa). The modified model provides an excellent description of forced-oscillation data for the newly prepared olivine polycrystal at temperatures of 900–1200 °C and oscillation periods of 1–1000 s, with a value of G_{UR} that is significantly (7%) less than the strictly anharmonic value for the same conditions (T_R,P_R). This modulus deficit is interpreted to reflect the impact of elastically accommodated grain-boundary sliding tentatively associated with a newly recognised 'plateau' with $Q^{-1} \sim 0.01$ that moves across the seismic band from long to short period with increasing temperature between 750 and 950 °C. The modified Burgers model is preferred over the Andrade-pseudoperiod and power-law Q^{-1} alternatives for its flexibility in specifying a distribution $D(\tau)$ of anelastic relaxation times that can account for both the monotonic background dissipation and the superimposed dissipation peak of elastically accommodated grain-boundary sliding, along with the associated modulus dispersion. Such 'background + peak' Burgers models, seamlessly describing the transition from (anharmonic) elasticity to grainsize-sensitive viscoelastic behaviour, have been fitted to the data for individual polycrystalline olivine specimens and suites of olivine polycrystals. Extrapolation of the model for our suite of essentially melt-free olivine polycrystals to mantle grain sizes and pressures suggest a significant contribution from grain-boundary relaxation under upper-mantle conditions. However, tighter constraints are expected from ongoing work-seeking confirmation of the occurrence at moderate temperatures of elastically accommodated sliding, and a cleaner separation of the roles of grainsize and water.

1. Introduction

The strong lateral variations in seismic wave speeds and attenuation in the Earth's upper mantle – including subduction-zone environments – are indicative of widespread viscoelastic relaxation of its constituent materials. Mechanisms of viscoelastic relaxation potentially responsible for reduced wave speeds and associated attenuation include grain-boundary processes, dislocation migration, both possibly enhanced by the presence of water, along with melt-related effects (melt squirt and the bulk relaxation arising from reversible stress induced melting/freezing) in partially molten material.

The inevitable frequency dependence of seismic properties of viscoelastic materials places a special premium on laboratory studies at seismic frequencies (e.g., Jackson et al., 2005). During the past decade, significant progress has been made in the study of seismic-wave attenuation in upper-mantle materials through low-frequency (mHz–Hz) torsional forced-oscillation measurements of fine-grained olivine polycrystals (Tan et al., 1997, 2001; Gribb and Cooper, 1998; Jackson et al., 2002; Cooper, 2003). Such materials, hot-pressed from either natural or fully synthetic precursors, possess generally low dislocation densities and are sufficiently fine-grained (d typically <30 μm) to be resistant to microcracking during thermal cycling at either atmospheric pressure (Cooper's laboratory) or the moderate confining pressure (0.2 GPa) of gas-medium high-pressure apparatus (ANU).

The experimental data comprise measurements of strain-energy dissipation Q^{-1} and the associated shear modulus G (not systematically reported by Cooper's group) as functions of

* Corresponding author. Fax: +61 2 6125 8253.
E-mail address: Ian.Jackson@anu.edu.au (I. Jackson).

0031-9201/$ – see front matter © 2010 Elsevier B.V. All rights reserved.
doi:10.1016/j.pepi.2010.09.005

oscillation period T_o, temperature T, and grainsize d, for (generally) dry polycrystalline specimens. In parallel experimental campaigns, the influence of a small melt fraction ϕ has also been documented (Gribb and Cooper, 2000; Jackson et al., 2004; Faul et al., 2004).

Such fine-grained materials, when tested in low-amplitude forced oscillation at sufficiently high temperature ($T > 800$–$900\,^{\circ}$C), show pronounced dispersion of the shear modulus (dependence upon frequency or oscillation period) and associated strain-energy dissipation—the twin manifestations of viscoelastic relaxation. The grainsize sensitivity of the viscoelastic relaxation observed in such materials of generally low dislocation density implicates intergranular rather than intragranular relaxation mechanisms.

Foremost amongst the candidate relaxation mechanisms for fine-grained materials is grain-boundary sliding. The classic theory of grain-boundary sliding, briefly reviewed in the next section, yields the following important prediction. The transition from elastic to viscoelastic behaviour caused by increasing temperature and/or oscillation period should begin with a dissipation peak attributed to sliding with elastic accommodation of grain-boundary incompatibilities. At higher temperatures and longer periods, the peak should merge into a broad dissipation background, associated with diffusionally accommodated sliding, in which the dissipation varies monotonically with temperature and period. As discussed in the next section, the predicted peak has been conspicuously absent from published experimental observations for genuinely melt-free materials—making it difficult to reconcile the growing body of extensive experimental data with apparently robust predictions of the theory.

It is the purpose of this paper to re-examine the transition from elastic, through anelastic, towards viscous behaviour through an experimental study of a newly prepared specimen of fine-grained melt-free olivine and to report circumstantial evidence for the predicted dissipation peak of elastically accommodated sliding. The new data have also been used to test alternative parameterisations (extended Burgers, and Andrade and power-law pseudoperiod functional forms) for the modelling of laboratory measurements of dispersion and dissipation. It is concluded that a variant of the extended Burgers model of Faul and Jackson (2005) is preferred for its flexibility in modelling dissipation consisting of both background and peak components along with the associated modulus dispersion. Its capacity to serve as an *interim* model for grainsize-sensitive viscoelastic relaxation for a suite of essentially melt-free olivines is then demonstrated. However, *definitive* analysis of the role of grain-boundary processes of viscoelastic relaxation in upper-mantle seismic wave dispersion and attenuation will require the tighter constraints on grainsize sensitivity and the role of water, expected to emerge from ongoing laboratory work.

2. Background: micro-mechanical models for viscoelastic relaxation associated with grain-boundary sliding

The transition from elastic to viscoelastic behaviour, ubiquitous in fine-grained polycrystalline materials exposed to shear stress at sufficiently high temperature, is usually attributed to grain-boundary sliding (e.g., Nowick and Berry, 1972). The incompatibilities in grain shape tending to arise from such relative displacement of adjacent grains are thought to be accommodated by appropriate elastic distortions of the individual grains (elastically accommodated grain-boundary sliding) and/or grain-boundary diffusion (diffusionally accommodated grain-boundary sliding). In the classic model of elastically accommodated grain-boundary sliding (Raj and Ashby, 1971), it is envisaged that the departure from elastic behaviour arises from slip on grain boundaries of low effective viscosity η_b within a two-dimensional array of regular hexagonal grains—at temperatures too low and timescales too short for appreciable diffusion. The Raj and Ashby analysis was based on the assumption of small slope (measured relative to the shear plane) for the periodic grain-boundary topography and its approximation by a truncated Fourier series. The limitation to small boundary slopes was overcome in the subsequent finite-element modelling of Ghahremani (1980).

The timescale for the anelastic relaxation associated with such elastically accommodated grain-boundary sliding is

$$\tau_e = \frac{\eta_b}{G_U \alpha_b}, \tag{1}$$

where $\alpha_b = \delta/d$ is the aspect ratio of the grain-boundary region of thickness δ for grain size d, and G_U is the unrelaxed shear modulus (Kê, 1947; Nowick and Berry, 1972; Mosher and Raj, 1974; O'Connell and Budiansky, 1977; Ghahremani, 1980). With their Fourier series representation of boundary topography truncated after 100 terms Raj and Ashby (1971) obtained a relaxation strength Δ of

$$\Delta = 0.57(1 - \nu) \tag{2}$$

i.e., 0.42 for Poisson's ratio $\nu = 0.26$ (as appropriate for olivine at 1000–1300 °C). A substantially lower value (0.23) of Δ was reported in the finite-element study of Ghahremani (1980). The relaxed shear modulus G_R and the height Q_D^{-1} of the Debye dissipation peak (as appropriate for the standard anelastic solid) are given by the following expressions:

$$\frac{G_R}{G_U} = \frac{1}{1+\Delta}; \quad Q_D^{-1} = \frac{(\Delta/2)}{(1+\Delta)^{1/2}}. \tag{3}$$

At higher temperatures and longer timescales, additional viscoelastic relaxation is expected to result from transient and steady-state diffusional creep. The transient required to adjust the normal stress distribution from that prevailing on completion of elastically accommodated sliding to that required for steady-state diffusional creep is of approximate duration:

$$\tau_d = \frac{(1-\nu)kTd^3}{40\pi^3 G_U \delta D_b \Omega}, \tag{4}$$

where Ω is the molecular volume of the diffusing species and D_b is the grain-boundary diffusivity (Raj, 1975). As noted by Gribb and Cooper (1998), τ_d differs from the Maxwell relaxation time $\tau_M = \eta_{SS}/G_U$ only by a multiplicative constant of order unity (where η_{SS} is the viscosity associated with steady-state diffusional creep). The transient creep rate (for timescales shorter than τ_d), calculated by Raj, is enhanced relative to the corresponding steady-state diffusional creep rate by a numerical factor that varies approximately as $(t/\tau_d)^{-1/2}$, which integrates to a creep function of the Andrade form (Eq. (15), below). Accordingly, the diffusional creep transient should be responsible for a wide viscoelastic absorption band, within which the dissipation Q^{-1} varies with oscillation period T_o and grain size d as (Gribb and Cooper, 1998; Faul et al., 2004):

$$Q^{-1} \sim T_o^{1/2} d^{-3/2} \tag{5}$$

The classic work of Raj and Ashby has recently been revisited by Morris and Jackson (2009a) in a study of sliding on a periodic model grain boundary that is the locus of *both* viscous sliding and diffusional transport of matter. Using a perturbation approach to solve the relevant boundary-value problem, they obtained an analytical solution (valid in the limit of infinitesimal boundary slope) for the *complete* mechanical relaxation spectrum, which for the case $\tau_e \ll \tau_d$, includes the following major features:

(a) a pronounced Debye-like dissipation peak at relatively short period $T_o \sim \tau_e$, that is associated with a marked reduction of the shear modulus, and is caused by elastically accommodated grain-boundary sliding;
(b) a broad region of very mild variation of Q^{-1} and G with period (and grain size) at intermediate periods ($\tau_e \ll T_o \ll \tau_d$), reflecting the fact that with increasing period, diffusion over progressively greater distances becomes more effective in relieving stress concentrations at relatively sharp grain corners;
(c) for periods $T_o > \tau_d$, the stronger (linear) variation of Q^{-1} with period appropriate for steady-state (Coble) creep.

The finding by Morris and Jackson (2009a) that the height of the elastically accommodated sliding peak varies inversely with (the infinitesimal) interfacial slope has subsequently been addressed in finite-element modeling of saw-tooth (S) and truncated saw-tooth (TS) boundaries of *finite* slope φ by Lee and Morris (2010). They have demonstrated that the peak height varies strongly and non-monotonically with interfacial slope. For a TS boundary with $\varphi = 60^\circ$ (Raj and Ashby, 1971, 'Mode 1') and an S boundary with $\varphi = 30^\circ$ (Raj and Ashby, 1971, 'Mode 2') with sharp corners modelled by effectively infinite Fourier series, the peak heights were found to be 0.040 and 0.047, respectively. The corresponding relaxation strengths Δ of 0.083 and 0.098 (Eq. (3)) for these two orthogonal modes of sliding sum to $\Delta = 0.181$ (i.e., $G_R/G_U = 0.85$) for a two-dimensional array of hexagonal grains—in reasonable accord with Ghahremani's (1980) finite-element result ($\Delta = 0.23$). Distributions of grainsize and grain-boundary viscosity (and presumably also boundary slope φ) in real polycrystalline materials both broaden and diminish the maximum amplitude of the dissipation peak (Lee and Morris, 2010).

The possibility, first suggested by Gribb and Cooper (1998) that high-temperature, seismic-frequency forced-oscillation data might belong to the regime of transient diffusonal creep (*b*, above) has recently been re-assessed by Morris and Jackson (2009b). They showed that the dissipation data for at least nominally melt-free olivine from both the ANU and the Cooper laboratories are consistent with a relationship of the form $Q^{-1} \sim F(X)$ with pseudoperiod master variable $X = T_o/(\eta_{SS}/G_U)$, without specifying the function F. The viscosity η_{SS} associated with steady-state diffusional creep came from independent creep measurements. It was therefore concluded that there is a single underlying relaxation mechanism with a characteristic time $\tau \sim \eta_{SS}/G_U$, i.e., τ_d.

However, full reconciliation of this interpretation with the theory of Raj and Ashby (and Morris and Jackson, 2009a) would require experimental observation of the dissipation peak of elastically accommodated sliding at lower values of the pseudoperiod X, i.e., shorter periods, coarser grainsize and/or lower temperatures. Despite intensive sampling of the experimental conditions appropriate for the transition from elastic to viscoelastic behaviour, particularly in the ANU work on melt-free olivine, there has so far been no compelling indication of the presence of the dissipation peak expected for elastically accommodated sliding. Similarly, many ceramic materials that lack a secondary grain-boundary phase of low viscosity show only a monotonic dissipation background and no clearly resolved dissipation peak. Instead, it has been argued that the presence of a dissipation peak superimposed upon the monotonic background appears to require the presence of a secondary phase of low viscosity, which may wet grain faces (e.g., silica glass in silicon nitride and silicon carbide) or be confined mainly to grain-edge tubules (e.g., basaltic melt in olivine) (Jackson et al., 2006).

3. Alternative empirical parameterisations of grain-size-sensitive viscoelastic relaxation

3.1. Extended Burgers model

The extended Burgers model of linear viscoelasticity with creep function:

$$J(t) = J_U \left\{ 1 + \Delta \int_{\tau_L}^{\tau_H} D(\tau) \left[1 - \exp\left(\frac{-t}{\tau}\right) \right] d\tau + \left(\frac{t}{\tau_M}\right) \right\} \tag{6}$$

was used (in slightly modified form—as discussed below) by Faul and Jackson (2005) to fit G and Q^{-1} data for a suite of melt-free olivine polycrystals and by Jackson (2005) to fit similar data for individual melt-bearing olivine specimens. The freedom to specify an appropriate distribution $D(\tau)$ of anelastic relaxation times provides the flexibility needed to describe both the smoothly monotonic background dissipation and any superimposed dissipation peak, and use of a creep function guarantees an internally consistent description of dissipation and modulus dispersion. In Eq. (6), J_U is the unrelaxed (infinite-frequency) compliance (strain/stress), Δ is the anelastic relaxation strength (being the fractional increase of compliance relative to J_U at $t = \infty$) and $\tau_M = \eta J_U$ is the Maxwell time for viscous relaxation.

The response of the extended Burgers model to sinusoidally time-varying stress is given by the dynamic compliance $J^*(\omega)$, which is essentially the Laplace transform of its creep function, with real and negative imaginary parts:

$$J_1(\omega) = J_U \left\{ 1 + \Delta \int_{\tau_L}^{\tau_H} \frac{D(\tau)\, d\tau}{(1+\omega^2\tau^2)} \right\} \tag{7a}$$

and

$$J_2(\omega) = J_U \left\{ \omega\Delta \int_{\tau_L}^{\tau_H} \frac{\tau D(\tau)\, d\tau}{(1+\omega^2\tau^2)} + \frac{1}{\omega\tau_M} \right\}, \tag{7b}$$

respectively. The shear modulus G and strain energy dissipation Q^{-1} are then calculable as functions of angular frequency $\omega = 2\pi/T_o$, or oscillation period T_o, by

$$G(\omega) = \left[J_1^2(\omega) + J_2^2(\omega)\right]^{-1/2} \tag{8a}$$

and

$$Q^{-1} = \frac{J_2(\omega)}{J_1(\omega)}. \tag{8b}$$

A distribution $D_B(\tau)$ of anelastic relaxation times that is commonly sufficiently flexible for modelling experimental data concerning the monotonic high-temperature background dissipation is

$$D_B(\tau) = \frac{\alpha\tau^{\alpha-1}}{(\tau_H^\alpha - \tau_L^\alpha)} \tag{9a}$$

with $0 < \alpha < 1$ for $\tau_L < \tau < \tau_H$, and zero elsewhere (Minster and Anderson, 1981).

Should it be necessary to model a dissipation peak superimposed upon the monotonic background, along with the associated dispersion, the distribution of anelastic relaxation times specified by Eqs. (9a) and (9b) can be augmented by the separately normalised distribution (Kampfmann and Berckhemer, 1985; Jackson, 2005):

$$D_P(\tau) = \sigma^{-1}(2\pi)^{-1/2} \exp\left\{ \frac{-[\ln(\tau/\tau_P)/\sigma]^2}{2} \right\} \tag{9b}$$

with relaxation strength Δ_P.

The lower (τ_L) and upper (τ_H) limits for the distribution of anelastic relaxation time, the 'peak' anelastic relaxation time τ_P and the Maxwell viscous relaxation time τ_M, are here referred to their respective values τ_{iR} (with i = L, H, P and M) under standard conditions of grain size d_R, temperature T_R and pressure P_R:

$$\tau_i(T,P,d)=\tau_{iR}\left(\frac{d}{d_R}\right)^m \exp\left[\left(\frac{E}{R}\right)\left(\frac{1}{T}-\frac{1}{T_R}\right)\right] \exp\left[\left(\frac{V}{R}\right)\left(\frac{P}{T}-\frac{P_R}{T_R}\right)\right]. \tag{10}$$

Potentially different values are allowed for the grain size exponents for anelastic (m_a for i = L, H, P) and viscous relaxation (m_v for i = M).

In their implementation of the extended Burgers model, Faul and Jackson (2005) refined the values of two parameters related to the unrelaxed compliance: $J_U(P)$ incorporating the well-established anharmonic pressure dependence, and $(\partial \ln J_U/\partial T)_R$. This latter parameter was used in prescription of the temperature sensitivity of J_U as

$$\delta \ln J_U(T) = \left(\frac{\partial \ln J_U}{\partial T}\right)_R \left(\frac{d}{d_R}\right)^{-mj} (T - T_R). \tag{11}$$

This approach was designed to capture not only the anharmonic temperature dependence, but also any (grain-size-sensitive) anelastic enhancement of $\partial G/\partial T$ resulting from relaxation at shorter periods than those of the high-temperature forced-oscillation experiments (i.e., <1 s for $T \geq 1000\,^\circ$C).

In an attempt to account *more explicitly* for all modulus relaxation beyond the elastic ideal, we have chosen to modify the previously employed parameterisation of the unrelaxed compliance J_U to incorporate its variation with temperature and pressure as

$$J_U(T,P) = \left[G_U(T_R,P_R) + (T - T_R)\frac{\partial G}{\partial T} + (P - P_R)\frac{\partial G}{\partial P}\right]^{-1}. \tag{12}$$

In using this strategy to fit experimental forced-oscillation data, we have set the reference pressure P_R = 0.2 GPa to be that of the forced-oscillation experiments, and the reference temperature T_R to 900 °C to correspond approximately with the onset of well-resolved anelastic relaxation in fine-grained polycrystalline olivine. In the first instance, $G_{UR} = G_U(T_R,P_R)$ is treated as an adjustable parameter, whereas $\partial G/\partial T$ and $\partial G/\partial P$ are either both constrained to the established anharmonic values, or $\partial G/\partial T$ is treated as adjustable. The value of G_{UR} thus determined is typically somewhat lower than the true unrelaxed value measured in ultrasonic or opto-acoustic studies at MHz–GHz frequencies (Section 4). This modulus deficit is attributed to elastically accommodated grain-boundary sliding, which is then modelled with a distribution of anelastic relaxation times modified according to Eq. (9b).

3.2. Andrade-pseudoperiod master variable approach

The Andrade-pseudoperiod strategy used by Jackson et al. (2004) to fit dissipation data for individual melt-free specimens is here extended to fit both Q^{-1} and G, potentially for a suite of melt-free materials, through use of the pseudo-period master variable:

$$X_B = T_o\left(\frac{d}{d_R}\right)^{-m} \exp\left[\left(\frac{-E_B}{R}\right)\left(\frac{1}{T}-\frac{1}{T_R}\right)\right] \exp\left[-\left(\frac{V}{R}\right)\left(\frac{P}{T}-\frac{P_R}{T_R}\right)\right] \tag{13}$$

in place of period T_o in $\omega = 2\pi/T_o$ in the following expressions for the real and negative imaginary parts of the dynamic compliance:

$$J_1(\omega) = J_U\left\{1 + \beta^* \Gamma(1+n)\omega^{-n} \cos\left(\frac{n\pi}{2}\right)\right\} \tag{14a}$$

$$J_2(\omega) = J_U\left\{\beta^* \Gamma(1+n)\omega^{-n} \sin\left(\frac{n\pi}{2}\right) + \frac{1}{\omega\tau_M}\right\} \tag{14b}$$

where Γ is the Gamma function. β^* and τ_M are related to the coefficients appearing in the usual expression for the Andrade creep function:

$$J(t) = J_U + \beta t^n + \frac{t}{\eta}, \tag{15}$$

by $\beta^* = \beta/J_U$, and $\tau_M = \eta J_U$ as for the Burgers model.

3.3. Power-law pseudoperiod master variable model for Q^{-1} only and calculation of the associated dispersion

Finally, we have also tested the performance of a power-law of the form:

$$Q^{-1} = AX^\alpha \tag{16}$$

(Jackson et al., 2002, Eq. (7)) with the controlling or 'master' variable X modified to refer the variations of grainsize, temperature and pressure to reference values d_R, T_R, and P_R, respectively, i.e.:

$$X = T_o\left(\frac{d}{d_R}\right)^{-1} \exp\left[\left(-\frac{E}{R}\right)\left(\frac{1}{T}-\frac{1}{T_R}\right)\right] \exp\left[-\left(\frac{V}{R}\right)\left(\frac{P}{T}-\frac{P_R}{T_R}\right)\right], \tag{17a}$$

which for the fitting of experimental data with $P = P_R$ becomes

$$X = T_o\left(\frac{d}{d_R}\right)^{-1} \exp\left[\frac{-(E + P_R V)(1/T - 1/T_R)}{R}\right]. \tag{17b}$$

The modulus dispersion associated with such power-law dissipation is given approximately by

$$\frac{G(T_o)}{G_U} = 1 - \cot\left(\frac{\alpha\pi}{2}\right) Q^{-1}(T_o) \tag{18}$$

provided that $Q^{-1} \ll 1$ (Brennan and Smylie, 1981; Minster and Anderson, 1981). Such conditions do not consistently apply to experimental data for fine-grained olivine where Q^{-1} approaches 1 for periods of 1000 s at 1200 °C. Accordingly, the strategy of fitting a power-law to the experimentally measured Q^{-1} data and approximating the associated dispersion with Eq. (18) is potentially problematic.

4. Comparative performance of the alternative strategies: sol–gel olivine 6585

Each of the alternative parameterisations of viscoelastic behaviour outlined in Section 3 has been fitted to a comprehensive set of unpublished torsional forced-oscillation data for a fine-grained synthetic Fo_{90} olivine polycrystal 6585. This dense specimen was hot-pressed for 24 h at 300 MPa and 1200 °C from powder prepared by a previously described solution-gelation procedure (Jackson et al., 2002). Its average grainsize of 3.1 μm was determined from an SEM backscattered electron image of an oxidised surface using the intercept method with a sectioning correction of $4/\pi$. Controlled-atmosphere firing of the precursor cold-pressed pellets and of the hot-pressed specimen at 1200–1400 °C resulted in material containing no water detectable by Fourier-transform infrared spectroscopy (i.e., <10 wt ppm H_2O). The specimen was hot-pressed and mechanically tested in torsional forced-oscillation within mild-steel jackets lined with $Ni_{70}Fe_{30}$ foil. The forced-oscillation tests were conducted as previously described (e.g., Jackson et al., 2002) but with the following *significant improvements* to the experimental methodology:

(a) use of a set of oscillation periods newly chosen to minimise the impact of the inevitable aliasing of mains-frequency (50 Hz)

noise that is under-sampled in the low-frequency records of displacement versus time from the forced-oscillation experiments;

(b) more intensive sampling of temperature-period space through consistent use of oscillation periods representative of the full experimentally accessible 3-decade range of oscillation period (1–1000 s), and 50 °C temperature intervals;

(c) application of a DC bias voltage to the electromagnetic drivers in order to minimise steady deformation resulting from any static torque transmitted through a vent tube connected to the lower end of the assembly. Such deformation leads to deterioration of transducer alignment and consequent drift and uncertainty in transducer sensitivity;

(d) use of a single layer of $Ni_{70}Fe_{30}$ foil (of 70 μm thickness) between specimen and the enclosing steel jacket, rather than a triple layer of foil, to minimise the uncertainty arising from our standard procedure of modelling the complex compliance of the foil as if it were mild steel, for which a comprehensive new experimental dataset has been employed.

Procedures for processing the forced-oscillation data have also been significantly improved as follows:

(i) An improved correction for a phase lag of electronic origin between the two displacement channels has eliminated an artificial tendency towards frequency-independent Q^{-1} at short periods and moderate/low temperatures.

(ii) Allowance has been made for the compliance of the frictional coupling between specimen and torsion rods by subtraction of the complex compliance of a 'double-foil' reference assembly (Jackson et al., 2009).

(iii) Use of a more realistic model for temperature and period-dependent viscoelastic behaviour of the Lucalox alumina control specimen (Jackson et al., 2009) has lowered the threshold value of Q^{-1} beyond which the dissipation can be robustly measured. The combined effect of these changes is that it becomes possible for the first time to make quantitative use of data for temperatures significantly less than 1000 °C, at least for the more lossy fine-grained materials, that provide new insight into the nature of the transition from elastic to anelastic behaviour.

4.1. Extended Burgers model

In an effort to minimise the number of adjustable parameters needed to adequately specify the extended Burgers model, the following strategy was employed. The interval $(\log \tau_{LR}, \log \tau_{HR})$ was specified as $(-2, 6)$ so that the absorption band just encompasses the 1–1000 s observational window for all temperatures in the range 900–1200 °C, for the optimal value of activation energy E. Concerning the unrelaxed shear modulus $G_U(T, P)$, $G_{UR} = G_U(T_R, P_R)$ is initially treated as an adjustable parameter, whereas $\partial G/\partial T$ and $\partial G/\partial P$ are normally each constrained to the established anharmonic values of $-13.6\,\mathrm{MPa\,K^{-1}}$ and 1.8 (Bass, 1995), respectively, but with the option of adjustable $\partial G/\partial T$. The values of the adjustable parameters G_{UR}, $[\partial G/\partial T]$, α, Δ_B, τ_{MR}, and E were refined by the Levenberg–Marquardt strategy for iterative non-linear least squares to minimise the objective function:

$$\chi^2 = \chi^2_G + \chi^2_{1/Q} \tag{19}$$

with $\sigma(G)/G = 0.03$ and $\sigma(\log Q^{-1}) = 0.05$. The latter expression is equivalent to a constant relative error $\sigma(Q^{-1})/Q^{-1} = 0.05 \times \ln 10 = 0.12$, and is preferred over the alternative of a fixed absolute error $\sigma(Q^{-1}) = 0.005$, that was also tested in this study.

The minimum value of χ^2 was obtained with both G_{UR} and $\partial G_U/\partial T$ treated as adjustable, but imposition of the anharmonic constraint on $\partial G_U/\partial T$ resulted in an acceptable χ^2 penalty of only 4% (Table 1). The viability of the purely anelastic Burgers model (with effectively infinite η or τ_M) was also tested—but found to increase χ^2 unacceptably by a further 56%. This observation resonates with the finding that $\log_{10}[\tau_M(\mathrm{s})]$ when refined, is well constrained at 5.2(1) for the preferred model highlighted in bold in Table 1. Comparison of the optimal Burgers model with the forced-oscillation data for specimen 6585 in Fig. 1(a) and (b) reveals an excellent overall fit with an average misfit $(\chi^2/2N)^{1/2}$ of 0.94 (Table 1).

The refined value of G_{UR} is somewhat lower (by 7%) than the true unrelaxed modulus obtained by anharmonic extrapolation from STP for fully dense pure Fo_{90} (66.5 GPa at $T_R = 900$ °C and $P_R = 0.2$ GPa). The possibility that such a discrepancy might be caused by a small amount (~1%) of porosity or inadequate correction for the compliance associated with the frictional coupling between specimen and torsion rods can be confidently discounted. This assertion is based on the observation that the 1–100 s averages of the shear moduli, robustly measured at 700 and 600 °C within the stability field for the low-temperature body-centred-cubic phase of the mild steel jacket, are within 1% of the corresponding anharmonic values.

However, close inspection of Fig. 1b reveals an apparently systematic departure from consistent power-law dependence of Q^{-1} upon oscillation period that develops on cooling below 1000 °C. This takes the form of a 'plateau' at $\log_{10} Q^{-1} = -1.85(3)$ for $\log T_o < 1.2$ and 950 °C, which moves systematically to longer periods with decreasing temperature: $\log_{10} Q^{-1} = -1.93(3)$ for $0.4 < \log_{10} T_o < 1.5$ at 900 °C, $\log_{10} Q^{-1} = -1.93(5)$ for $0.7 < \log_{10} T_o < 2.1$ at 850 °C, and $\log_{10} Q^{-1} = -1.99(2)$ for $1.5 < \log T_o$ for 800 °C. Further cooling (below 800 °C) results in generally much lower and more scattered values of Q^{-1} within the 1–1000 s band, accompanied by a substantial increase in shear modulus. The capacity to resolve the transition from significantly anelastic behaviour for $\log_{10} T_o > 1.5$ at $T \geq 800$ °C to essentially elastic behaviour for $1 < \log_{10} T_o < 3$ and $T \leq 700$ °C is complicated somewhat by the sluggish kinetics of the fcc–bcc transition and consequent uncertainty in the viscoelastic properties of the mild steel jacket during cooling across the temperature interval ~870–710 °C (Jackson et al., 2000).

This moderate-temperature plateau, newly observable because of the previously described improvements in experimental technique and data processing, plausibly represents the superposition on an otherwise monotonically positive $\log_{10} Q^{-1}(\log_{10} T_o)$ trend of a modest dissipation peak attributable to elastically accommodated sliding. A *Debye peak* of height 0.01 would be associated with an anelastic relaxation strength Δ of 0.02 and accordingly a 2% relaxation of the shear modulus (Eq. (3)). However, larger values of Δ, and therefore more modulus relaxation, would be associated with a broader peak of the same height.

In this way, the shear modulus data for specimen 6585 can simultaneously be reconciled with the anharmonic value for G_{UR} and the presence of the poorly resolved dissipation plateau near $Q^{-1} = 0.01$, by augmentation of the distribution of anelastic relaxation time through Eq. (9b). A satisfactory outcome (Fig. 1c and d) is obtained by fixing G_{UR} at its anharmonic value and the peak width parameter (Eq. (9b)) σ at 4, and refining the values of Δ_P and $\log \tau_{PR}$, with common activation energy and activation volume for the background and peak-related relaxations (Table 1). The significance of this result is that the extended Burgers model with the modified distribution of relaxation times reconciles the viscoelastic behaviour observed at sub-Hz frequencies seamlessly with the unrelaxed modulus measured at MHz–GHz frequencies with ultrasonic and opto-acoustic techniques.

Table 1
Alternative Burgers, Andrade and power-law strategies for the representation of G and Q^{-1} data[a] derived from torsional forced-oscillation measurements for fine-grained olivine polycrystal 6585. The data consist of (G,Q^{-1}) data pairs for uniformly spaced oscillation periods between 1 and 1000 s and temperatures of 800–1200 °C, at maximum shear strain amplitudes of 10^{-6} to 10^{-5}.

Burgers[b]	G_{UR} (GPa)	$\partial G_U/\partial T$ (MPa/K)	Δ_B	α	$\log\tau_{LR}$	$\log\tau_{HR}$	$\log\tau_{MR}$	E (kJ/mol)	χ^2_G	$\chi^2_{1/Q}$	χ^2	$(\chi^2/2N)^{1/2}$
	62.8(5)	−19(3)	1.5(1)	0.33(1)	[−2]	[6]	5.1(1)	293(8)	31.3	81.7	112.9	
	62.0(3)	**[−13.6]**	**1.4(1)**	**0.33(1)**	**[−2]**	**[6]**	**5.2(1)**	**303(8)**	**35.6**	**81.8**	**117.4**	**0.94**
	61.8(3)	[−13.6]	2.0(1)	0.38(1)	[−2]	[6]	[10]	290(7)	42.4	141.2	183.5	
Burgers[c]	**[66.5]**	**[−13.6]**	**1.4(1)**	**0.33(1)**	**[−2]**	**[6]**	**5.4(1)**	**327(7)**	**48.4**	**130.5**	**178.9**	**1.06**

Andrade	G_{UR} (GPa)	$\partial G_U/\partial T$ (MPa/K)	β^* (s^{-n})	n	$\log\tau_{MR}$	E (kJ/mol)	χ^2_G	$\chi^2_{1/Q}$	χ^2	$(\chi^2/2N)^{1/2}$
	63.0(5)	−19(3)	0.020(1)	0.33(1)	5.2(1)	295(8)	31.3	81.7	113.0	
	62.2(3)	**[−13.6]**	**0.020(1)**	**0.33(1)**	**5.3(1)**	**303(8)**	**35.7**	**81.8**	**117.5**	**0.94**
	62.0(3)	[−13.6]	0.016(1)	0.37(1)	[10]	296(7)	40.8	125.2	166.0	

Power-law	G_{UR} (GPa)	$\partial G_U/\partial T$ (MPa/K)	A (s^{-n})	α	E (kJ/mol)	χ^2_G	$\chi^2_{1/Q}$	χ^2	$(\chi^2/N)^{1/2}$
	–	–	**68(12)**	**.34(1)**	**293(9)**	**–**	**88.7**	**88.7**	**1.16**

[a] Except for the Burgers background + peak model[c], $N = 66$ (G,Q^{-1}) data pairs, representing the temperature interval 1200–900 °C inclusive, were employed (Four (G,Q^{-1}) pairs for low-loss conditions—1.28 s period at 950 °C and 1.28–6.4 s at 900 °C being excluded). For the Burgers background + peak model[d], all 1–1000 s data for 900–1200 °C were fitted—along with the most coherent 12–214 s data at 850 °C and 47–1000 s data at 800 °C (thus $N = 80$). Other parameter values: $d_R = 3.1$ μm, $T_R = 900$ °C (1173 K), $P_R = 0.2$ GPa, $V = 10 \times 10^{-6}$ m^3 mol^{-1}; $G_U(T_R,P_R) = 66.5$ GPa, $\partial G/\partial P = 1.8$, $\partial G_U/\partial T = -13.6$ MPa K^{-1}, $\sigma(G)/G = 0.03$, $\sigma(\log Q^{-1}) = 0.05$.
[b] Background only (Eq. (9a)).
[c] Background + peak (Eqs. (9a), (9b) and (10)) with $\Delta_P = 0.07(1)$, $\log\tau_{PR} = -2.9(2)$, $\sigma = [4]$, and common activation energy and activation volume for the background and peak-related relaxations.

Finally, it should also be noted that experimental data over a limited frequency range are inevitably unable to resolve the trade-off between the specified width of the anelastic absorption band (τ_L, τ_H) and the relaxation strength Δ_B which is the fractional increment in compliance associated with complete (i.e., $t = \infty$) anelastic relaxation.

4.2. Andrade pseudo-period model

The *Andrade* model, with its implicit infinitely wide distribution of anelastic relaxation times, is superficially attractive for its parametric economy relative to the Burgers model. Without the need to specify the interval (τ_L,τ_H), and with fixed anharmonic $\partial G/\partial T$, the Andrade fit to G and Q^{-1} data for a material of given grainsize involves just 5 parameters $G_U(T_R,P_R)$, n, β^*, τ_{MR}, and E. Comparison of the Andrade and extended Burgers models in Table 1 and Fig. 1 reveals essentially identical fits to the same experimental data for specimen 6585. That the value of the parameter n in the Andrade model is identical with that of α in the Burgers model indicates that it plays the same role in setting the functional form of the distribution of anelastic relaxation times—implicit within the Andrade model. Similarly, the parameter $\beta^* = \beta/J_U$ in the Andrade model, like Δ_B in the extended Burgers model, is a measure of the anelastic relaxation strength. That the Andrade model is parametrically economical relative to the extended Burgers model is attributable to its use of an implicit distribution of anelastic relaxation times that is infinitely wide–obviating the need to specify τ_L and τ_H. The result, however, is undesirable asymptotic behaviour: infinite creep rate $(dJ/dt = n\beta t^{n-1} + 1/\eta)$ for $t \to 0$ and the persistence of transient creep, albeit at diminishing importance relative to steady-state creep, as $t \to \infty$ (e.g., Jackson, 2000).

4.3. Power-law $Q^{-1}(T_o)$ model

The extended Burgers and Andrade models each prescribe a variation of Q^{-1} with period that closely approximates a power law within the anelastic absorption band. It is therefore unsurprising that a power-law (Eq. (16)) fits the Q^{-1} data almost as well as the other two models (Table 1). The exponent α for the optimal power-law model is essentially identical in value to the parameters α and n of the extended Burgers and Andrade models, respectively, and the activation energies E are also closely comparable amongst all three models. Although the power-law model thus provides a reasonable approximation to the experimental $Q^{-1}(T_o,T)$ data, calculation of the associated dispersion of the shear modulus is straightforward only for the restrictive condition $Q^{-1} \ll 1$. Indeed, it is evident from the results plotted in Fig. 1g and h that Eq. (18) is a useful approximation to the dispersion measured for fine-grained olivine specimen 6585 only for $\log_{10} Q^{-1} < -1$.

4.4. Summary

Amongst the three models investigated, only the extended Burgers model provides the flexibility to model the variations of both G and Q^{-1} with an explicit distribution of anelastic relaxation times that can readily be modified to describe departures of the dissipation from the uniform monotonic background $(Q^{-1} \sim T_o^{\alpha})$ associated with $D(\tau) \sim \tau^{\alpha-1}$ (Eq. (9a)). We have shown how $D(\tau)$ can be modified to accommodate additional viscoelastic relaxation, plausibly attributed to elastically accommodated grain-boundary sliding, for which there is circumstantial evidence in both the G and Q^{-1} data. Such an approach, involving incorporation of an additional log-normal distribution of anelastic relaxation times has previously proved effective in the modelling of a Q^{-1} peak superimposed upon the monotonic background for melt-bearing olivine (Jackson, 2005).

5. Application of the preferred Burgers strategy to other essentially melt-free olivine polycrystals

5.1. Individual specimens

The preferred extended Burgers model, initially without modification to include elastically accommodated sliding, has been newly applied to previously published forced-oscillation data for each of the essentially melt-free specimens in the ANU suite (Tan et al., 2001; Jackson et al., 2002, 2004). Such data pre-date the improvements to the experimental methodology described in Section 4, but have been re-processed to take advantage of the new strategy for data analysis. The Q^{-1} data become progressively more noisy and scattered as $\log_{10} Q^{-1}$ decreases towards and beyond −2. Data for relatively low temperatures and short periods have there-

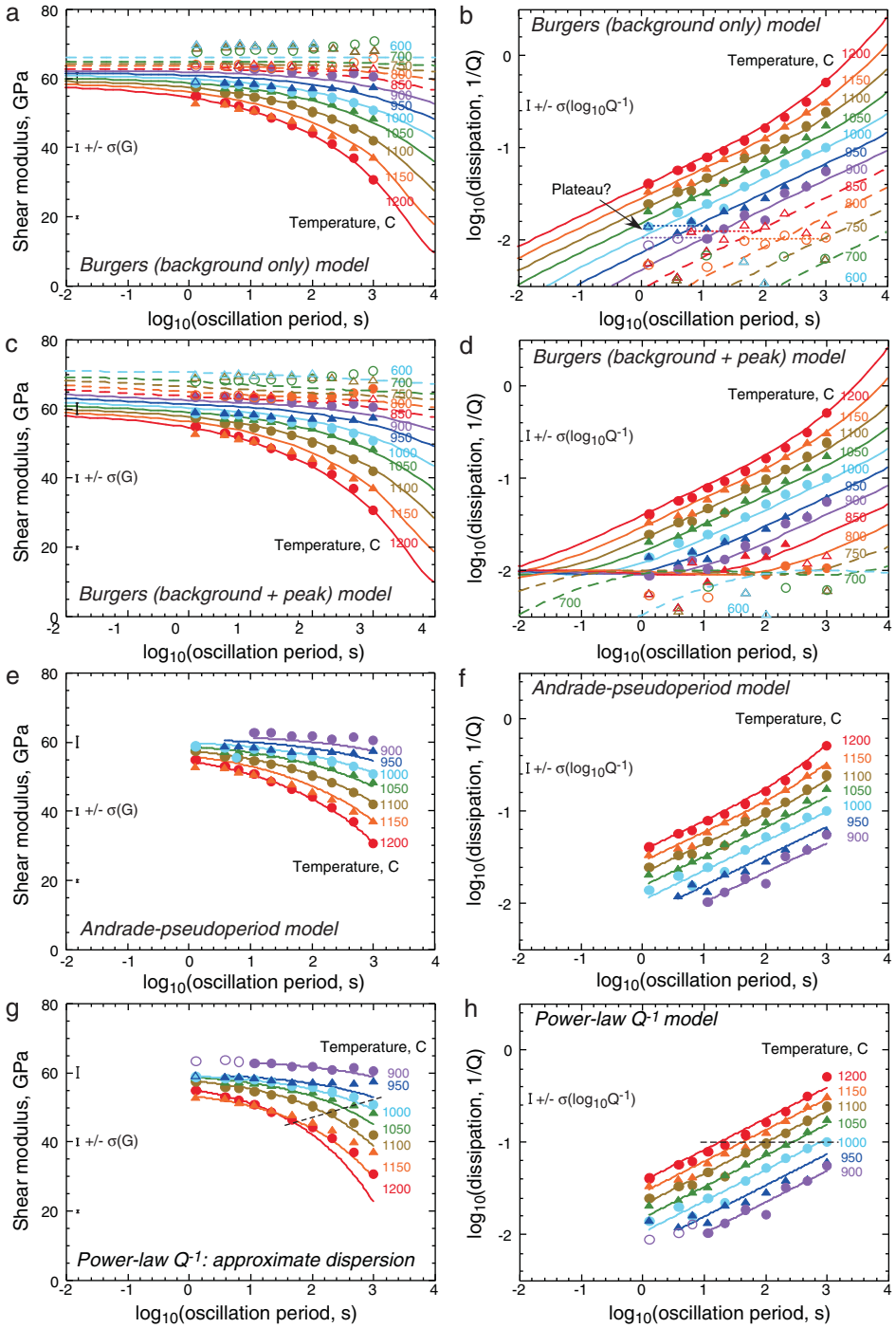

Fig. 1. Comparison of the alternative models (Table 1, curves) with the torsional forced-oscillation data (plotting symbols) for fine-grained Fo_{90} olivine polycrystal 6585. Solid symbols identify the subset of data used to constrain each of the models. The uncertainties in shear modulus ($\sigma(G)/G = 0.03$) and dissipation ($\sigma(\log_{10} Q^{-1}) = 0.05$) are indicated by the error bars on the left-hand side of each panel. (a and b) Burgers (background-only) model fitted to the $N = 66$ dataset (Table 1, footnote a), with the postulated Q^{-1} plateau highlighted. (c and d) Burgers (background + peak) model fitted to the expanded $N = 80$ dataset (Table 1, footnote a). (e and f) Andrade pseudoperiod model fitted to the $N = 66$ dataset. (g and h) Power-law model (Eq. (16)) fitted to the $N = 66$ dataset with dispersion calculated through Eq. (18). The $Q^{-1} \ll 1$ approximation underpinning Eq. (18) breaks down for $\log_{10} Q^{-1} > -1$, this threshold being indicated by the broken lines.

fore been systematically excluded from the dataset employed to constrain the model—as documented in the notes associated with Table 2. Guided by the experience with specimen 6585 above, we have constrained $\partial G_U/\partial T$ to its anharmonic value, and fixed a priori the width (τ_{LR}, τ_{HR}) of the anelastic absorption band at the reference conditions $[T_R, P_R, (d_R)]$, for all further modelling. The values of all parameters of the optimal models, including the five refined by iterative least-squares $[G_U(T_R, P_R), \alpha, \Delta_B, [\tau_{MR}]$, and $E]$ are assembled in Table 2.

For the three most coarse-grained specimens, the values of $G_{UR} = G_U(T_R, P_R)$ closely approach (within 3–4%) the anharmonic value of 66.5 GPa, whereas for the two most fine-grained specimens the modulus deficits are 7 and 10% for specimens 6585 and 6381, respectively. As discussed previously, the most likely explanation for the deficit involves anelastic relaxation occurring for periods of 1–1000 s at lower temperatures than those for which the model is constrained. Each of the datasets except 6328 contains evidence suggestive of the presence of a poorly resolved plateau with

Table 2
Comparison of Burgers fits[a] of forced-oscillation data[b] for essentially melt-free olivine specimens.

	d (μm)	N	T (°C)	G_{UR} (GPa)	Δ_B	α	log τ_{LR} (s)	log τ_{HR} (s)	log τ_{MR} (s)	E (kJ/mol)	Δ_P	log τ_{PR} (s)	σ	$(\chi^2/2N)^{1/2}$
Individual specimens														
6381	2.9	41[c]	1000–1200	59.9(4)	0.7(1)	0.29(1)	[−2]	[6]	5.7(1)	392(18)				1.09
		52[d]	800–1200	[66.5]	0.78(7)	0.28(1)	[−2]	[6]	5.7(1)	400(14)	0.10(1)	−4.4(2)	[4]	1.17
6585	3.1	66[e]	900–1200	62.0(3)	1.4(1)	0.33(1)	[−2]	[6]	5.2(1)	303(8)				0.94
		80[f]	800–1200	[66.5]	1.4(1)	0.33(1)	[−2]	[6]	5.4(1)	327(7)	0.07(1)	−2.9(2)	[4]	1.06
6365	12.4	34[g]	800–1200	63.9(4)	1.3(2)	0.26(1)	[−3]	[7]	[7]	300(16)				1.15
		33[h]	800–1200	[66.5]	1.6(3)	0.29(2)	[−3]	[7]	[7]	322(17)	0.049(6)	−3.1(3)	[4]	0.93
6261	23.4	33[i]	800–1200	63.9(4)	0.34(3)	0.13(1)	[−3]	[7]	5.6(3)	367(30)				1.37
		33[j]	800–1200	[66.5]	0.36(4)	0.15(1)	[−3]	[7]	5.9(3)	394(32)	0.041(6)	−5.1(4)	[4]	1.32
6328	165.1	12[k]	900, 1200	64.4(6)	0.19(7)	0.17(4)	[−3]	[7]	6.0(6)	370(70)				1.17

	N	m_a	G_{UR} (GPa)	Δ_B	α	log τ_{LR} (s)	log τ_{HR} (s)	log τ_{MR} (s)	E (kJ/mol)	Δ_P	log τ_{PR} (s)	σ	$(\chi^2/2N)^{1/2}$
Multiple sol–gel specimens													
6381, 6585, 6365[l]	141	0.69(6)	61.9(2)	1.9(1)	0.29(1)	[−3]	[7]	5.8(1)	310(6)				1.31
6381, 6585, 6365[m]	165	0.88(7)	[66.5]	1.9(1)	0.30(1)	[−3]	[7]	6.12(6)	348(6)	0.072(3)	−3.7(1)	[4]	1.26
6381, 6585, 6365[n]	165	0.93(7)	[66.5]	1.9(1)	0.30(1)	[−3]	[7]	5.71(6)	347(6)	0.072(3)	−3.7(1)	[4]	1.26
All essentially melt-free specimens													
6381, 6585, 6365, 6261, 6328[o]	180	1.19(4)	62.5(2)	1.13(6)	0.257(5)	[−3]	[7]	6.95(5)	303(6)				1.54
6381, 6585, 6365, 6261, 6328[p]	**204**	**1.31(4)**	**[66.5]**	**1.04(5)**	**0.274(5)**	**[−3]**	**[7]**	**7.48(5)**	**360(6)**	**0.057(2)**	**−3.4(1)**	**[4]**	**1.41**
6381, 6585, 6365, 6261, 6328[q]	204	1.32(4)	[66.5]	1.04(5)	0.274(5)	[−3]	[7]	6.40(5)	360(6)	0.057(2)	−3.4(1)	[4]	1.41

[a] For background-only fits (Eq. (9a)), the values of $G_{UR} = G(T_R,P_R)$, $[\partial G/\partial T]$, α, Δ_B, log τ_{MR}, and E were refined while log τ_{LR} and log τ_{HR} were held fixed as indicated by the square parentheses. Other parameter values: $T_R = 900$ °C, $P_R = 0.2$ GPa, $V = 10 \times 10^{-6}$ m^3 mol^{-1}; $G_U(T_R,P_R) = 66.5$ GPa, $\partial G_U/\partial T = -13.6$ MPa K^{-1}, $\partial G/\partial P = 1.8$, $\sigma(G)/G = 0.03$, $\sigma(\log Q^{-1}) = 0.05$. For background + peak fits (Eqs. (9a) and (9b)), the additional parameters Δ_P and log τ_{PR} were refined with σ held fixed, using common activation energy and activation volume for the background and peak-related relaxations.

[b] Previously published data for specimens other than 6585 have been reprocessed with the improved procedures described in the text.

[c] Published data for 1–1000 s period have been replaced by data obtained at 1–100 s period following further annealing at 1200 °C prior to staged cooling. All data for 1000–1200 °C included.

[d] As for note (c) but with data with $\log_{10} Q^{-1} > -2.25$ at 800 and 900 °C also included, except for the outlier at 100 s and 900 °C.

[e] $N = 66$ dataset, from Table 1.

[f] $N = 80$ dataset, From Table 1.

[g] Data for 1.024 s period at 800 °C excluded.

[h] All 1–100 s data for 800–1200 °C with $\log Q^{-1} > -2.25$ were fitted.

[i] Data for 1300 °C and $T_o > 30$ s at 1200 °C excluded.

[j] Same exclusions as note (i) with lowest $\log Q^{-1} = -2.31$.

[k] Data for 1–50 s period at 1200 °C and 1–100 s at 900 °C only.

[l] All data used in such fits for individual specimens; $d_R = 4.8$ μm, $m_v = 3$.

[m] All data used in such fits for individual specimens with $d_R = 4.8$ μm, $m_v = 3$.

[n] As for note (m) but with the constraint $m_v = m_a$.

[o] All data used in such fits for individual specimens, but with 900 °C data for 6328 excluded; $d_R = 13.4$ μm, $m_v = 3$.

[p] All data used in such fits for individual specimens with $d_R = 13.4$ μm, $m_v = 3$.

[q] As for note (p) but with the constraint $m_v = m_a$.

$-2.0 > \log_{10} Q^{-1} > -2.2$ within the observational period range at 800 °C (Fig. 3). As discussed above for specimen 6585, the presence of such a Q^{-1} plateau along with a modest modulus deficit plausibly results from the superposition of a small peak associated with elastically accommodated grain-boundary sliding upon the otherwise consistently monotonic background dissipation, attributed to further, diffusionally accommodated, sliding. Accordingly, the dataset for each individual specimen, expanded where necessary to include essentially all data for $T \geq 800$ °C and $\log_{10} Q^{-1} > -2.3$ (see notes below Table 2 for details), have been fitted to the extended Burgers model with a distribution $D(\tau)$ of anelastic relaxation times modified to incorporate a broad dissipation peak and associated modulus dispersion attributable to elastically accommodated sliding. The optimal fits are compared with the corresponding background-only models in Table 2. The average misfit $(\chi^2/2N)^{1/2}$ is increased by only 7 and 13% for the significantly enlarged datasets for specimens 6381 and 6585, respectively. For specimens 6365 and 6261, the average misfit *decreases* by 19 and 4%, respectively, with the modification of $D(\tau)$.

The relatively coarse-grained and therefore not very dissipative specimen 6261, when tested at temperatures of 1200–1300 °C and periods greater than 10–30 s, shows an unphysical negative dependence of Q^{-1} upon period, probably resulting from overestimation of the (complex) compliance associated with the frictional coupling between specimen and torsion rods. With such data excluded, we obtained adequate fits to the remaining 33 (G,Q^{-1}) pairs for the temperature interval 800–1200 °C. The uncertainty concerning the correction for the compliance of frictional coupling is greatest for the most coarse-grained ($d = 165.1$ μm) and low-loss specimen 6328. However, the six (G,Q^{-1}) pairs for $T_o < 50$ s at 1200 °C with $-1.4 > \log Q^{-1} > -2.0$ provide an indicative benchmark for its viscoelastic behaviour. The Q^{-1} data obtained at lower temperatures are generally too widely scattered to be useful, but the 900 °C data have been included only to allow an estimate of the activation energy.

5.2. Towards a global model

The values of the key parameters for different specimens are sufficiently consistent or systematically variable with grainsize as to suggest the possibility of a global fit to all of the data. Continuing with the same broad strategy (minimising the number of free parameters by fixing a priori the position of the anelastic absorption band (τ_{LR}, τ_{HR}) and constraining $\partial G_U/\partial T$ to its anharmonic value) we therefore now seek to incorporate the grain-size sensitivity.

In the first instance, this has been done with a *background-only Burgers model*, refining the value of the grain-size exponent m_a for the lower and upper bounds (τ_L, τ_H) on the distribution of anelastic relaxation times. For this purpose, the corresponding exponent m_v for the Maxwell (viscous) relaxation time, which is actually very poorly constrained by our existing forced-oscillation dataset, was fixed at 3(2) as appropriate for Coble (Nabarro-

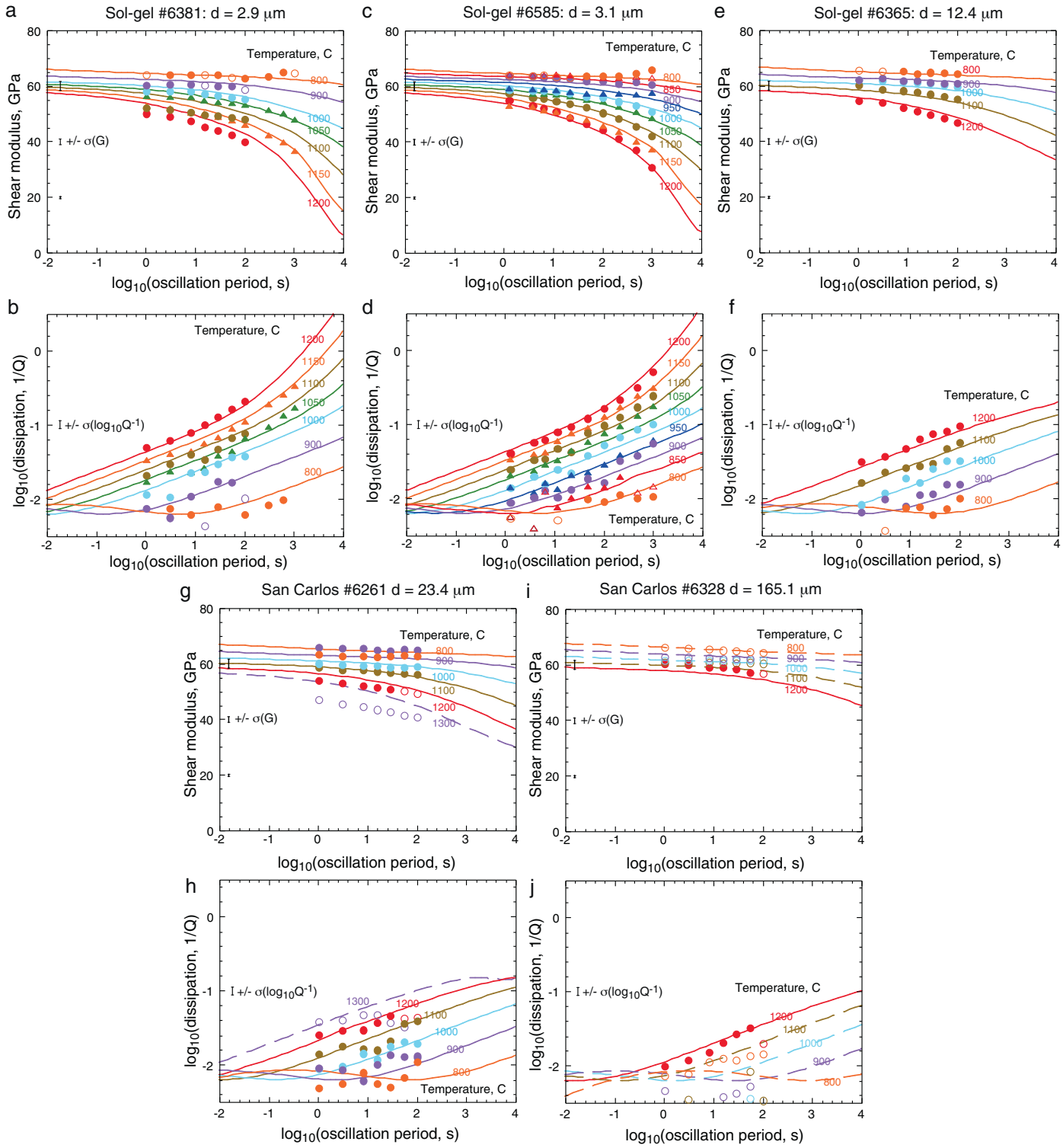

Fig. 2. Comparison between forced-oscillation data and the grainsize-sensitive background + peak Burgers model fitted to 204 (G,Q^{-1}) data pairs for essentially melt-free sol–gel specimens 6381, 6585, 6365 and San Carlos specimens 6261 and 6328 (Table 2). The plotting symbols and error bars have the same significance as in Fig. 1.

Herring) creep controlled by grain-boundary (lattice) diffusion. '*Background + peak*' *models*, for which the grainsize exponent m_a also controls the grainsize sensitivity of τ_{PR}, have also been tested. Finally, as an alternative, consistent with the notion of a single pseudoperiod master variable, we have also tested the possibility that $m_a = m_v$.

5.2.1. Grainsize-sensitive relaxation in dry, genuinely melt-free sol–gel olivine

Broadly satisfactory Burgers model fits are obtained when the data for the most intensively studied sol–gel specimen 6585 are combined with those for both of the other sol–gel derived specimens 6381 and 6365. Simultaneous modelling of the data for

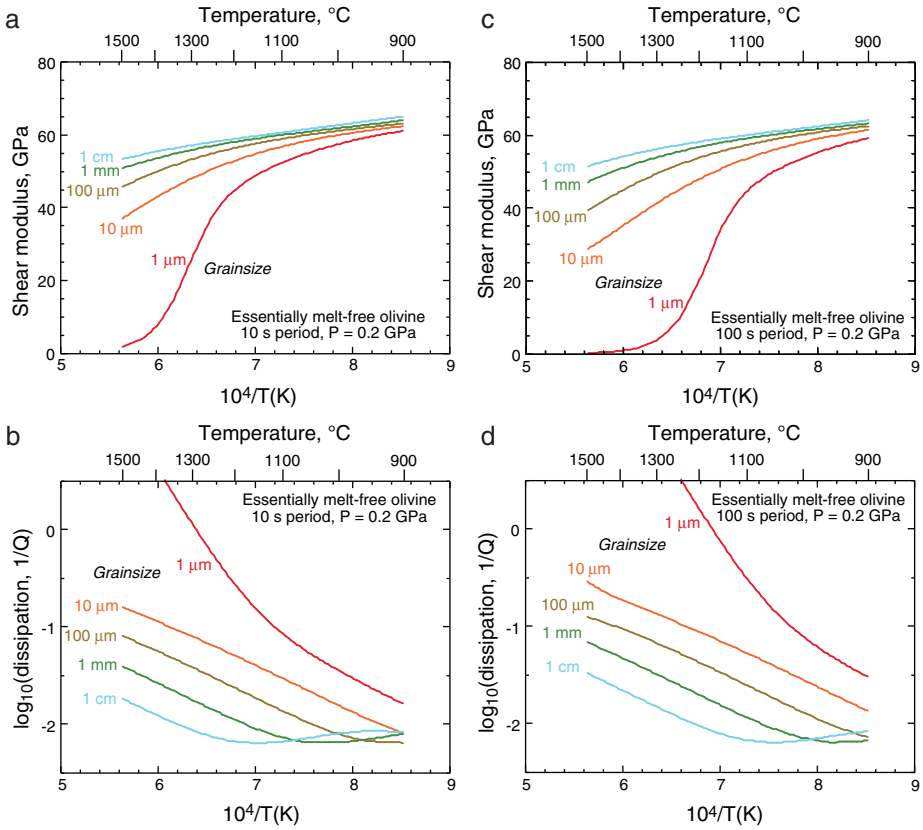

Fig. 3. Extrapolation of the interim Burgers (background + peak) model for essentially melt-free olivine (Table 2, note (p)) to conditions of grainsize and temperature representative of teleseismic wave propagation in the Earth's upper mantle—highlighting the grainsize sensitivity at each of two representative oscillation periods, 10 s (a and b) and 100 s (c and d). For the extrapolation in pressure, see Fig. 4.

all three of these specimens provides redundancy for $d \sim 3$ μm, and the significantly more coarse-grained specimen 6365 provides some constraint on the grainsize sensitivity (Table 2). The grainsize sensitivity of the anelastic relaxation times thus inferred is mild with $m_a \sim 0.7$ for the background-only fit and 0.9 for the background + peak fit.

Specimen 6381 is somewhat more compliant than 6585 at 1100–1200 °C (Fig. 2), possibly reflecting lesser microstructural maturity associated with a shorter annealing period at 1200 °C prior to final data acquisition, but the data for the two ~3 μm specimens are otherwise very similar. The ~3 μm specimens tested to 1000 s period at temperatures >1000 °C display significant upward curvature in their $Q^{-1}(T_o)$ trends that results from a progressively larger viscous contribution to Q^{-1} with increasing period, as noted previously. However, the grainsize sensitivity of $\tau_M \sim d^{mv}$ with $m_v = 3$ is much stronger than that ($m_a \sim 0.7$–0.9) inferred for τ_L, τ_H and τ_P. The effect is to reverse the curvature of the $Q^{-1}(T_o)$ trends between $d = 3$ and $d = 12.4$ μm. The optimal fits of Table 2 are essentially unchanged by making the alternative a priori choice $m_v = 2$ for Nabarro-Herring creep, or by imposing the constraint $m_a = m_v$ (Table 2).

5.2.2. Implications for the broader suite of sol–gel and San Carlos specimens

On account of their greater chemical complexity, the specimens prepared from the natural precursor material and recovered by staged cooling from maximum temperatures of 1200–1300 °C contain small volume fractions (<0.1%) of silicate melt (Tan et al., 2001; Jackson et al., 2004). Moreover, early in our experimental campaign, both precursor cold-pressed pellets and hot-pressed specimens precision-ground for mechanical testing were sometimes oven-dried rather than being consistently fired at 1200–1400 °C. Accordingly, the early specimens 6261, 6328 and 6365 contain appreciable concentrations of mainly molecular water (130, 35–70 and 75 wt ppm H_2O, respectively), whereas water is below the FTIR detection limit (10 wt ppm) in the later specimens 6381 and 6585.

The predictions of the sol–gel model derived in the previous section for the appropriate grainsizes have been compared with the data for San Carlos specimens 6261 and 6328. The more coarse-grained of these specimens (6328, $d = 165.1$ μm) is significantly less compliant and lossy than extrapolation of the sol–gel model would suggest, whereas specimen 6261 ($d = 23.4$ μm) is more closely comparable.

Accordingly, we have constructed a new interim model for essentially melt-free olivine (c.f. Faul and Jackson, 2005) constrained by the forced-oscillation data for the suite of intensively studied fine-grained sol–gel specimens 6381, 6585 and 6365 along with the sparser data for the more coarse-grained San Carlos specimens 6261 ($T \leq 1200$ °C) and 6328 (1200 °C only). The resulting model, which is insensitive to the choice of m_v ($m_v = 3$, or 2, or constrained to be equal to m_a), is compared with data for all five specimens in Fig. 2. It is a broadly satisfactory fit to all of the constraining data. The most significant outliers are the 1300 °C data for 6261, possibly affected by the presence of melt.

The optimal Burgers background-only fit to the data for our essentially melt-free specimens involves a value of $G_{UR} = G_U(T_R, P_R) = 62.5$ GPa which is 6% lower than the anharmonic value for the same conditions. This modulus deficit is similar to that (7%) for the most intensively studied specimen 6585, but substantially less than the ~15% modulus relaxation expected from the finite-element calculations of Lee and Morris (2010) for elastically accommodated sliding in a two-dimensional array of regular hexagonal 'grains'. As for the individual specimens and the sol–gel suite, we have also examined the alternative

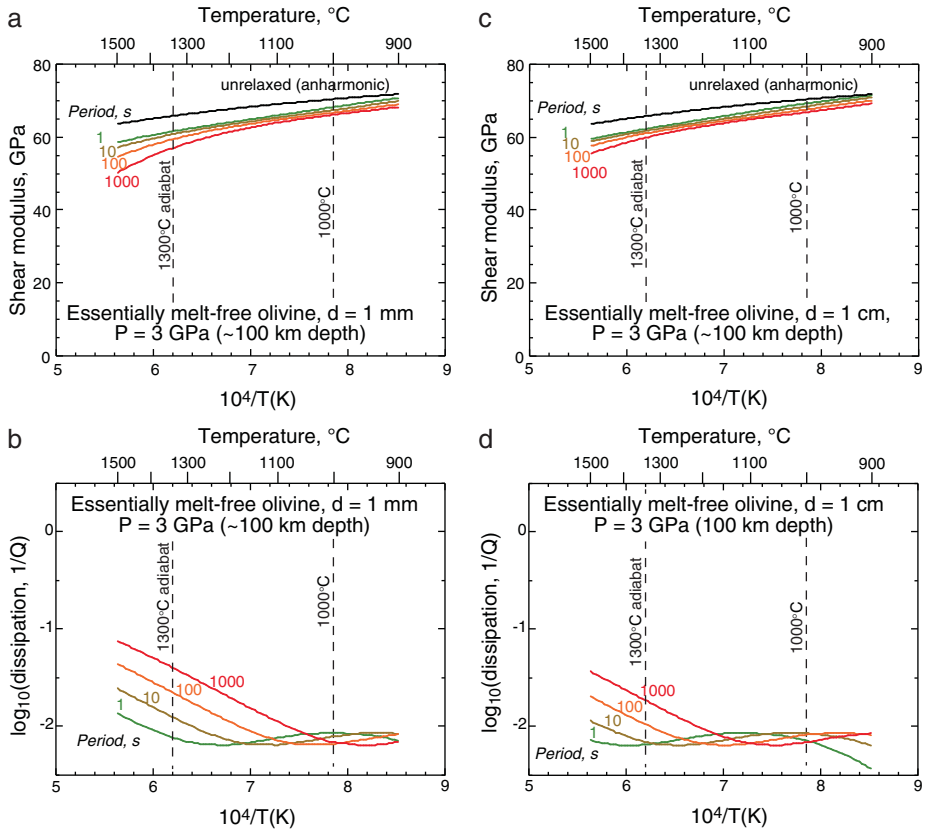

Fig. 4. Extrapolation of the interim Burgers (background + peak) model for essentially melt-free olivine (Table 2, note (p)) to conditions of grainsize, temperature and pressure (3 GPa) representative of teleseismic wave propagation at a depth of 100 km in the Earth's upper mantle—highlighting the sensitivity to seismic shear-wave period at each of two representative grain sizes, 1 mm (a and b) and 1 cm (c and d). The black curves in panels (a) and (c) indicate the unrelaxed (anharmonic) temperature dependence of the shear modulus.

background + peak model, involving strictly anharmonic $G_U(T,P)$ and a modified distribution $D(\tau)$ of anelastic relaxation times.

The models of Table 2 for the essentially melt-free specimens involve a grainsize sensitivity (e.g., $m_a = m_v = 1.3$) that is somewhat stronger than that for the sol–gel suite (e.g., $m_a = m_v = 0.9$). While exponents ~1 are reasonable for elastically accommodated grain-boundary sliding (Eq. (1)), larger exponents of 2 or 3 are expected for viscoelastic relaxation attributable to diffusionally accommodated grain-boundary sliding (Gribb and Cooper, 1998; Cooper, 2003; Morris and Jackson, 2009b). It is possible that the grainsize sensitivity may have been underestimated if water were playing a role (e.g., Karato, 2003; Aizawa et al., 2008) by selectively enhancing the viscoelastic relaxation in the wetter, more coarse-grained specimens of the ANU suite. Additional data from work in progress on dry, nearly melt-free specimens of grain size ≥ 20 μm, preferably involving improved coupling between specimen and torsion rods and a more nearly elastic reference assembly, will help tighten the constraints on the grainsize sensitivity, and also begin to clarify the role of water.

6. Implications for the interpretation of seismological models

The forced-oscillation experiments are performed at teleseismic frequencies and at temperatures closely approaching those of the Earth's upper mantle. However, the pressure routinely accessible in the ANU gas-medium high-pressure apparatus is only 0.2 GPa, and grainsizes have been limited to the range 3–160 (but mainly <25 μm) in order to minimise the influence of microcracking during thermal cycling. So, significant extrapolations in both grain size and pressure are required for seismological application of our new, interim laboratory-based model.

6.1. Extrapolation to mantle grain size

The Burgers background + peak model fitted to the (G,Q^{-1}) data for the suite of five essentially melt-free olivine specimens (Table 2, $m_v = 3$ fit) has accordingly firstly been evaluated at the reference pressure $P_R = 0.2$ GPa, teleseismic periods of 1–1000 s, and temperatures of 900–1500 °C, for grainsizes ranging between 1 μm and 1 cm. The dissipation Q^{-1} and shear modulus dispersion each decrease systematically, but mildly, with increasing grain size (Fig. 3).

6.2. Extrapolation in pressure

The higher pressures in the Earth's upper mantle than in the laboratory experiments influence the values of G and Q^{-1} calculated from the Burgers model in two ways: through the pressure derivative $\partial G/\partial P$ of the unrelaxed modulus (Eq. (12)) and through the effect of the activation volume V on the relaxation times (Eq. (10)). With an indicative value $V = 10 \times 10^{-6}$ m^3 mol^{-1} (c.f. Faul and Jackson, 2005), the estimated relaxation times increase 8.1-fold with *increasing* pressure from $P_R = 0.2$ GPa to $P = 3$ GPa (~100 km depth) at the representative temperature (1340 °C ($10^4/T$(K) ~ 6.2) for this depth in the convecting upper mantle (e.g., Katsura et al., 2004). Thus at, mm–cm grain size, periods of 1–1000 s, and temperatures along the 1300 °C adiabat, grainsize-sensitive relaxation processes in melt-free olivine are expected to make a significant contribution to the seismologically observed attenuation—at

the level of $-2.2 < \log_{10} Q^{-1} < -1.3$ (Fig. 4). In this regime, Q^{-1} varies approximately as the 1/4 power of period, and displays an Arrhenian dependence upon temperature, as appropriate for the high-temperature background associated with diffusionally assisted grain-boundary sliding. However, for mm–cm grainsize and temperatures below 1100 °C, as expected for sub-cratonic lithosphere, the $\log Q^{-1} \sim -2.1$ plateau associated with elastically accommodated grain-boundary sliding results in nearly frequency- and temperature-independent attenuation (Fig. 4d).

7. Conclusions and prospects

A newly prepared dry, melt-free olivine specimen of ~3 μm grain size, has been intensively tested in torsional forced oscillation at high temperatures with improved experimental protocols and procedures for data analysis. Its microstrain viscoelastic behaviour at teleseismic periods of 1–1000 s displays the following features in order of increasing temperature: (i) a poorly resolved $\log_{10} Q^{-1} \sim -1.9(1)$ plateau at 800–900 °C and 1–1000 s period, accompanied by a modulus relaxation of ~7%, marking the onset of appreciably anelastic rheology; (ii) a broad regime (900–1100 °C) of consistent power–law variation of dissipation with period: $Q^{-1} \sim T_o^{\alpha}$ with $\alpha \sim 1/4$ and associated modulus dispersion; (iii) markedly stronger period sensitivity of Q^{-1} at long periods for $T > 1100$ °C signalling the onset of a gradual transition from anelastic towards viscous behaviour.

The shear modulus and dissipation data for regimes (ii) and (iii) are equally well described by extended Burgers and Andrade pseudoperiod models. However, the former provides the flexibility of an explicit distribution $D(\tau)$ of anelastic relaxation times that can be readily modified to suit more complex relaxation spectra involving superposition of a dissipation peak upon a uniformly monotonic dissipation background, as required, for example, to account for the plateau of regime (i). The dissipation data for regime (ii) are adequately described by a power-law variation with oscillation period, but the associated dispersion is well described by the low-loss approximation only for $\log_{10} Q^{-1} < -1$.

The observation of an admittedly poorly resolved Q^{-1} plateau at moderate temperature helps reconcile these experimental observations with micro-mechanical models of grain-boundary sliding, if the dissipation peak responsible for the observed Q^{-1} plateau is attributed to elastically accommodated sliding. The inferred peak height ~0.01 and modulus relaxation (7%) are both significantly lower, and the peak is broader, than predicted by the finite-element modelling of two-dimensional arrays of regular hexagonal 'grains' of Ghahremani (1980) and Lee and Morris (2010). These differences may reflect the presence in real materials of distributions of grainsize and boundary viscosity (Lee and Morris, 2010) and boundary slope.

The extended Burgers (background + peak) model fitted to data for the ANU suite of five fine-grained, essentially melt-free olivine polycrystals, suitably extrapolated in grainsize and pressure, suggests that grain-boundary relaxation processes may contribute significantly to seismic wave dispersion and attenuation under upper-mantle conditions. However, robust interpretation of seismological models will depend upon ongoing work promising a cleaner separation of the relative influence of variations in grain size and water content.

Acknowledgements

We are grateful to colleagues whose interest in our forced-oscillation data and questions about our Burgers model have encouraged us to think more deeply about the modelling of grainsize-sensitive viscoelastic relaxation, especially Reid Cooper, John Fitz Gerald, Greg Hirth, Stephen Morris, Doug Wiens and Slava Solomatov. Harri Kokkonen, Craig Saint and Robert Farla are thanked for assistance with the fabrication and characterisation of the synthetic polycrystalline olivine. The manuscript was significantly improved in response to thoughtful reviews by Marshall Sundberg and an anonymous reviewer.

References

Aizawa, Y., Barnhoorn, A., Faul, U.H., Fitz Gerald, J.D., Jackson, I., Kovács, I., 2008. Seismic properties of Anita Bay dunite: an exploratory study of the influence of water. J. Petrol. 49, 841–855, doi:10.1093/petrology/egn007.

Bass, J.D., 1995. Elasticity of minerals, glasses and melts. In: Ahrens, T.J. (Ed.), Mineral Physics and Crystallography, A Handbook of Physical Constants. American Geophysical Union, Washington, USA, pp. 45–63.

Brennan, B.J., Smylie, D.E., 1981. Linear viscoelasticity and dispersion in seismic wave propagation. Rev. Geophys. Space Phys. 19 (2), 233–246.

Cooper, R.F., 2003. Seismic wave attenuation: energy dissipation in viscoelastic crystalline solids. In: Karato, S., Wenk, H. (Eds.), Reviews in Minerology and Geochemistry: Plastic Deformation in Minerals and Rocks. Mineralogical Society of America, Washington, pp. 253–290.

Faul, U.H., Fitz Gerald, J.D., Jackson, I., 2004. Shear-wave attenuation and dispersion in melt-bearing olivine polycrystals. Part II. Microstructural interpretation and seismological implications. J. Geophys. Res 109, B06202, doi:10.1029/2003JB002407.

Faul, U.H., Jackson, I., 2005. The seismological signature of temperature and grain size variations in the upper mantle. Earth Planet. Sci. Lett. 234, 119–134.

Ghahremani, F., 1980. Effect of grain boundary sliding on anelasticity of polycrystals. Int. J. Solids Struct. 16, 825–845.

Gribb, T.T., Cooper, R.F., 1998. Low-frequency shear attenuation in polycrystalline olivine: grain boundary diffusion and the physical significance of the Andrade model for viscoelastic rheology. J. Geophys. Res. 103 (B11), 27267–27279.

Gribb, T.T., Cooper, R.F., 2000. The effect of an equilibrated melt phase on the shear creep and attenuation behaviour of polycrystalline olivine. Geophys. Res. Lett. 27 (15), 2341–2344.

Jackson, I., 2000. Laboratory measurements of seismic wave dispersion and attenuation: recent progress. In: Karato, S., et al. (Eds.), Earth's Deep Interior: Mineral Physics and Tomography from the Atomic to the Global Scale. AGU Geophys. Monogr. Ser., vol. 117, pp. 265–289.

Jackson, I., 2005. Laboratory measurement of seismic wave dispersion and attenuation at high pressure and temperature. In: Chen, J., Wang, Y., Duffy, T.S., Shen, G., Dobrzhinetskaya, L. (Eds.), Advances in High-Pressure Technology for Geophysical Applications. Elsevier, pp. 95–119.

Jackson, I., Barnhoorn, A., Aizawa, Y., Saint, C., 2009. Improved experimental procedures for the study of high-temperature viscoelastic relaxation. Phys. Earth Planet. Inter. 172, 104–115.

Jackson, I., Faul, U.H., Fitz Gerald, J.D., Morris, S.J.S., 2006. Contrasting viscoelastic behaviour of melt-free and melt-bearing olivine: implications for the nature of grain-boundary sliding. Mater. Sci. Eng. A 442, 170–174.

Jackson, I., Faul, U.H., Fitz Gerald, J.D., Tan, B.H., 2004. Shear-wave attenuation and dispersion in melt-bearing olivine polycrystals. I. Specimen fabrication and mechanical testing. J. Geophys. Res. 109, B06201, doi:10.1029/2003JB002406.

Jackson, I., Fitz Gerald, J.D., Faul, U.H., Tan, B.H., 2002. Grainsize sensitive seismic wave attenuation in polycrystalline olivine. J. Geophys. Res. 107 (B12), 2360, doi:10.1029/2001JB001225.

Jackson, I., Fitz Gerald, J.D., Kokkonen, H., 2000. High-temperature viscoelastic relaxation in iron and its implications for the shear modulus and attenuation of the Earth's inner core. J. Geophys. Res. 105, 23605–23634.

Jackson, I., Webb, S.L., Weston, L., Boness, D., 2005. Frequency dependence of elastic wave speeds at high-temperature: a direct experimental demonstration. Phys. Earth Planet. Inter. 148, 85–96.

Kampfmann, W., Berckhemer, H., 1985. High temperature experiments on the elastic and anelastic behaviour of magmatic rocks. Phys. Earth Planet. Inter. 40, 223–247.

Karato, S., 2003. Mapping water content in the upper mantle. In: Eiler, J. (Ed.), The Subduction Factory, Geophysical Monograph 138. AGU, Washington, pp. 135–152.

Katsura, T., Yamada, A., Kubo, T., Shinmei, T., Nishikawa, O., Yoshino, Y., Aizawa, Y., Song, M.S., Walter, M.J., Ito, E., Funakoshi, K., 2004. Olivine–wadsleyite transition in the system $(Mg,Fe)_2SiO_4$. J. Geophys. Res. 109, B02209, doi:10.1029/2003JB002438.

Kê, T., 1947. Experimental evidence of the viscous behaviour of grain boundaries in metals. Phys. Rev. 71 (8), 533–546.

Lee, L.C., Morris, S.J.S., 2010. Anelasticity and grain boundary sliding. Proc. Roy. Soc. A. 466, 2651–2671.

Minster, J.B., Anderson, D.L., 1981. A model of dislocation-controlled rheology for the mantle. Phil. Trans. Roy. Soc. Lond. 299, 319–356.

Morris, S.J.S., Jackson, I., 2009a. Diffusionally-assisted grain-boundary sliding and viscoelasticity of polycrystals. J. Mech. Phys. Solids 57, 744–761.

Morris, S.J.S., Jackson, I., 2009b. Implications of the similarity principle relating creep and attenuation in finely-grained solids. Mater. Sci. Eng. A 521–522, 124–127.

Mosher, D.R., Raj, R., 1974. Use of the internal friction technique to measure rates of grain boundary sliding. Acta Metall. 22, 1469–1474.
Nowick, A.S., Berry, B.S., 1972. Anelastic Relaxation in Crystalline Solids. Academic, New York, 677 pp.
O'Connell, R.J., Budiansky, B., 1977. Viscoelastic properties of fluid-saturated cracked solids. J. Geophys. Res. 82, 5719–5735.
Raj, R., 1975. Transient behaviour of diffusion-induced creep and creep rupture. Metall. Trans. A 6A, 1499–1509.
Raj, R., Ashby, M.F., 1971. On grain boundary sliding and diffusional creep. Metall. Trans. 2, 1113–1127.
Tan, B.H., Jackson, I., Fitz Gerald, J.D., 1997. Shear wave dispersion and attenuation in fine-grained synthetic olivine aggregates: preliminary results. Geophys. Res. Lett. 24 (9), 1055–1058.
Tan, B.H., Jackson, I., Fitz Gerald, J.D., 2001. High-temperature viscoelasticity of fine-grained polycrystalline olivine. Phys. Chem. Miner. 28, 641–664.